Patra *et al. Geoscience Letters* (2026) 13:27
https://doi.org/10.1186/s40562-026-00476-z

Geoscience Letters

RESEARCH Open Access

Recent increase in N_2O growth rate (2013–2023) mainly due to increase of nitrogen-fertiliser and manure use in the Northern Tropics and Southern Landmass

Prabir K. Patra[1,2,3*], Yasunori Tohjima[4], Akihiko Ito[5], Naveen Chandra[1], Motoki Sasakawa[4], Xin Lan[6,7], Bradley D. Hall[6], Paul B. Krummel[8], Ray F. Weiss[9], Christina M. Harth[9], Shinya Takatsuji[10], Daisuke Goto[11], Kumiko Takata[1,13], Luke M. Western[12] and Ronald G. Prinn[12]

Abstract
Nitrous oxide (N_2O) is a strong greenhouse gas that contributes significantly to global warming and causes depletion of ozone in the stratosphere. Recent observational records show an unprecedented acceleration in atmospheric N_2O growth, reaching 1.15 ppb yr^{-1} in 2019–2023, a significant increase compared to 0.68 ppb yr^{-1} in 2001–2005. This surge in growth rate is particularly pronounced over tropical regions, and has been measured most prominently at the southern-most island of Japan (Hateruma). In this study, we use N_2O observations from globally distributed multi-institutional networks and the MIROC4-ACTM inversion framework to quantify N_2O emissions and identify key regions that are driving the recent acceleration. Our results suggest that the major Asian countries, Brazil, Central and Northern Africa, and the Contiguous United States have increased emission sources in the recent 2.5 decades (1998–2023). Further, there has been an increase in land N_2O emissions, at a rate of 106 GgN yr^{-1} per year during 1998–2002 to 2019–2023 (1Gg = 10^9g). The inversion inferred trends are consistent with increased fertiliser use and manure production to support extensive agriculture, and terrestrial ecosystem model results. The emissions from oceanic regions did not show significant increases in N_2O (rate: 7 ± 2 GgN yr^{-1} per year) in our inverse model setup. Our results underscore the importance for improved climate mitigation strategies and emissions reduction policies by increasing nitrogen-fertiliser use efficiency in agricultural land.

Keywords Nitrous oxide, N_2O emissions, Chemistry-transport model, Regional source-sink inversion, Nitrogen fertiliser, Natural soil, Oceanic exchange, Ecosystem nitrogen dynamics

Bradley D. Hall: Retired from NOAA/GML.

*Correspondence:
Prabir K. Patra
prabir@jamstec.go.jp

Full list of author information is available at the end of the article

© The Author(s) 2026. **Open Access** This article is licensed under a Creative Commons Attribution 4.0 International License, which permits use, sharing, adaptation, distribution and reproduction in any medium or format, as long as you give appropriate credit to the original author(s) and the source, provide a link to the Creative Commons licence, and indicate if changes were made. The images or other third party material in this article are included in the article's Creative Commons licence, unless indicated otherwise in a credit line to the material. If material is not included in the article's Creative Commons licence and your intended use is not permitted by statutory regulation or exceeds the permitted use, you will need to obtain permission directly from the copyright holder. To view a copy of this licence, visit http://creativecommons.org/licenses/by/4.0/.

Introduction

Nitrous oxide (N_2O) is a long-lived greenhouse gas (GHG) with an atmospheric lifetime of approximately 109 ± 10 years and global warming potential of 273 at 100 year time horizon (Forster et al. 2021). Since preindustrial times, its concentration has risen from ~270 parts per billion (ppb) in 1750 to 336.69 ± 0.03 ppb in 2023, contributing significantly to both climate change and stratospheric ozone depletion (Rubino et al. 2019; Lan et al. 2025; Canadell et al. 2021; WMO/SAOD 2022). The current rate of increase is estimated at ~3.3% per decade during 2014–2023 (Prinn et al. 2018; Lan et al. 2025), driven primarily by microbial nitrification and denitrification in terrestrial and aquatic ecosystems. These microbial processes are influenced by environmental and biological factors, including soil moisture, temperature, oxygen availability, soil acidity, and nitrogen substrate levels (Porporato et al. 2003; Butterbach-Bahl et al. 2013; Bouwman et al. 2013; Tian et al. 2024; Zhu et al. 2025a, b). Anthropogenic activities—such as synthetic fertilizer use, livestock manure management, industrial emissions, and waste treatment—contribute substantially to the global N_2O budget (Thompson et al. 2019; Crippa et al. 2024; Ito et al. 2018), with emissions expected to rise in response to increasing global demands for food, feed, fiber and energy as per the assessment of the United Nations (UNEP/FAO 2024; Tubiello et al. 2022; Cui et al. 2021) and under climate change (Harris et al. 2022; Li et al. 2024; Vitousek et al. 1997).

Global N_2O emissions have increased from about 10.5 TgN yr^{-1} (1 Tg = 10^{12} g) in the preindustrial era to ~17.0 TgN yr^{-1} in the decade 2007–2016, with agriculture as the dominant driver (Prather et al. 2015; Canadell et al. 2021). Agricultural N_2O emissions increased from 0.3 to 1.0 TgN yr^{-1} in 1861 to 3.9–5.3 TgN yr^{-1} by 2015, as estimated by the N_2O Model Intercomparison Project (NMIP) (Tian et al. 2018). Given the urgency of limiting non-CO_2 GHG emissions to achieve climate targets, effective N_2O mitigation strategies must reduce emissions without compromising food security. This underscores the importance of enhancing nitrogen use efficiency (NUE)—optimizing the fraction of nitrogen uptake by crops relative to nitrogen inputs—and adopting sustainable agricultural practices. Therefore, continuous monitoring of atmospheric N_2O growth and identifying key drivers are critical for informed mitigation policies. Further large gaps persist among the estimated emissions of N_2O by the terrestrial ecosystem models, inverse modelling of atmospheric data and the national reports (Del Grosso et al. 2022; Tian et al. 2024).

Recent observational records reveal an acceleration in atmospheric N_2O growth rates since 2000, increasing from 0.68 ppb yr^{-1} (2001–2005) to 0.98 ppb yr^{-1} (2010–2015), reaching about 1.15 ppb yr^{-1} in the most recent years (2019–2023) (Lan et al. 2025). This recent surge is particularly pronounced over tropical regions, marking an unprecedented rise in the past two decades and suggesting the agricultural practices and NUE dynamics may have changed regionally. In this study, we utilize global N_2O observation networks and the MIROC4-ACTM inversion framework at JAMSTEC (Patra et al. 2022) to quantify N_2O emissions and identify key regions driving the recent surge in atmospheric N_2O levels. This inverse model is one of the 4 models currently providing emission estimations to the Global N_2O Budget (Tian et al. 2024; Thompson et al. 2019).

Methods

Atmospheric observations

We use observations from the National Oceanic & Atmospheric Administration (NOAA), Advanced Global Atmospheric Gases Experiment (AGAGE), Commonwealth Scientific and Industrial Research Organisation (CSIRO), National Institute for Environmental Studies (NIES), and Japan Meteorological Agency (JMA) (Huang et al. 2008; Prinn et al. 2018; Lan et al. 2024; Tojima et al. 2020; Takatsuji 2025). Some of the 49 sites have overlapping measurements from more than one institution (Table S1; Fig. 1d), with the number of unique sites at 40. Data from the NOAA, CSIRO and JMA sites are reported on the NOAA-2006 A calibration scale (also referred to as WMO_N2O_X2006A), while the NIES and AGAGE data are reported on the independent scales of NIES and SIO-2016, respectively (Hall et al. 2007). Co-located measurements from AGAGE (SIO-2016) and NOAA (NOAA-2006 A) at five common sites show site-dependent and time-dependent differences, amounting to ~0.5 ppb and ~0.2 ppb in the late 1990s and early 2020s, respectively. To account for the scale differences, we subtracted a fixed value of 0.5 ppb from the AGAGE data. We added 0.6 ppb to the NIES data, consistent with a -0.6 ppb offset relative to NOAA identified in WMO/IAEA Round Robin Comparison #6 (2014–2015) (https://gml.noaa.gov/ccgg/wmorr/wmorr_results.php?rr=rr6&param=n2o; last accessed 02 September 2025). We performed sensitivity inversion experiments to assess the time-dependent SIO-2016 vs. NOAA-2006 A scale difference, NOAA/AGAGE = 4.3641×10^{-5} * Year + 0.91065 (Fig. S1).

Most of the measurement sites are located away from the emission hotspots seen in Fig. 1c but due to coarse transport model simulations at about 2.8° × 2.8° horizontal resolution (details in Sect. 2.2), simulations for some of the sites are affected by emission hotspots. Due to the presence of multiple sites in such cases, e.g., at TAP (site#28 in Fig. 1) in East Asia, and by assigning lower weightage of the sites (greater data uncertainty), the effect of single sites has been found to be negligible on

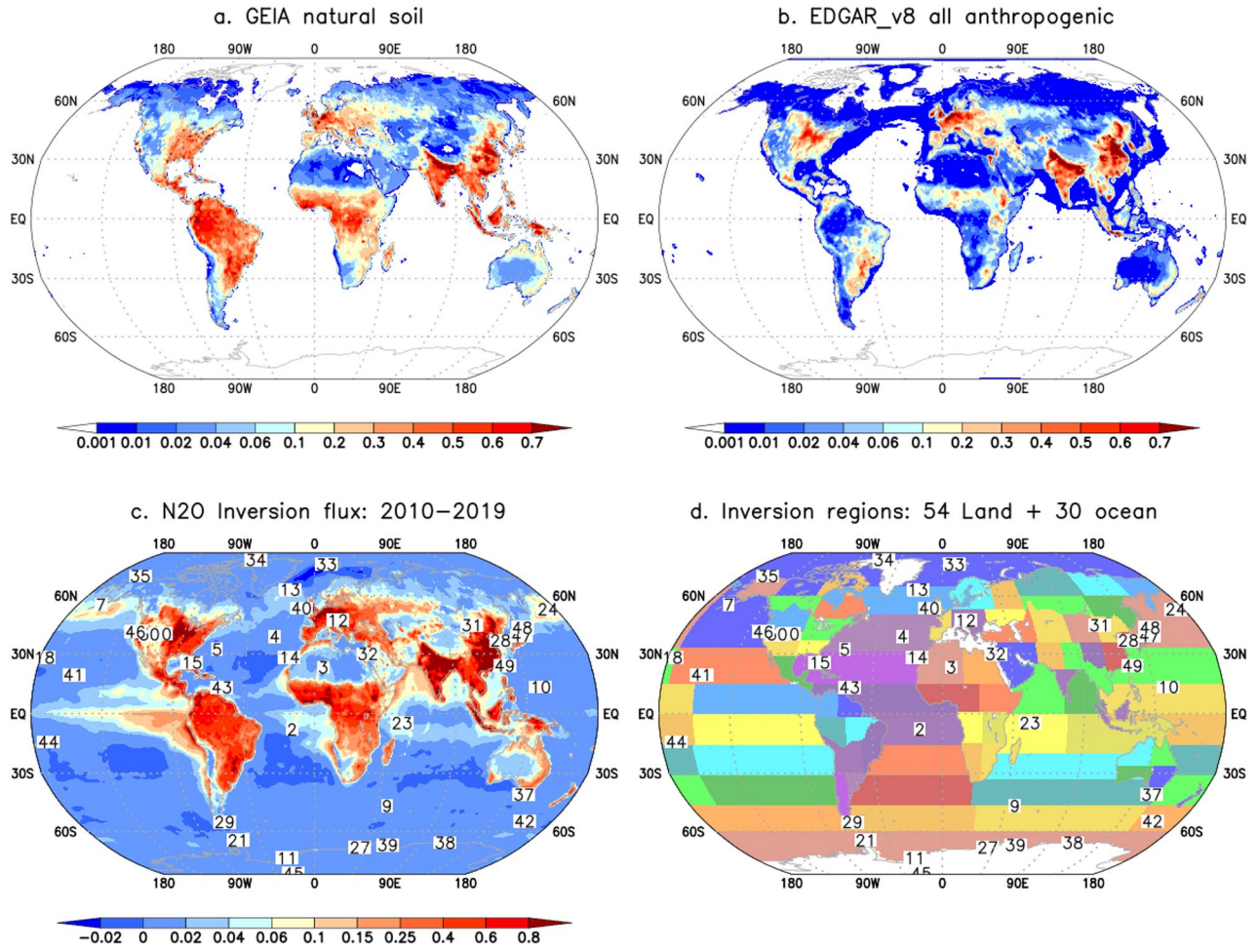


Fig. 1 Maps of the Global Emission Initiative (GEIA) natural soil emissions (**a**), annual mean emissions from industrial and agricultural activities from the Emissions Database for Global Atmospheric Research, version 8 (EDGAR_v8) for 2010–2019 (**b**), total N_2O fluxes estimated by MIROC-ACTM inverse model averaged over 2010–2019 (**c**). Location of 49 measurement sites (marked by the numbers) used in the inversion are shown on top of 84 inverse model regions (**d**). The inverse model has 30 regions over the ocean and 54 regions over the land (Patra et al. 2022)

inversion analyses. Similar to Patra et al. (2022), all the time series, observations and model simulations for the sites, are passed through a Butterworth bandpass filter with cutoff length of 24 months and fitted with 6 harmonics before using them in the inversion system (following Nakazawa et al. 1997).

Atmospheric N_2O forward and inverse models

The setups of our forward chemistry and transport for N_2O simulation by MIROC4-ACTM have been discussed in Patra et al. (2018, 2024), and thus only a brief description is given here. The atmospheric general circulation model MIROC, version 4 is developed by the University of Tokyo, NIES and JAMSTEC (Watanabe et al. 2010). The MIROC4-ACTM meteorology is nudged toward the JMA's 55-year Reanalysis (JRA-55; Kobayashi et al. 2015). We use MIROC4-ACTM at T42 horizontal resolution (42 spectral truncation) and 67-layer hybrid vertical coordinates. The lifetime of N_2O in MIROC4-ACTM is about 127 years, which is in the range of the estimations by various assessment reports (Prather et al. 2015; Canadell et al. 2021; Burkholder and Hodnebrog 2023). The model transport properties in representing the Brewer-Dobson circulation and stratosphere-stratosphere exchange processes in MIROC4-ACTM using JRA-55 meteorology have been tested using multiple chemical tracers (Patra et al. 2018; Bisht et al. 2021).

We optimise fluxes from 84 partitions of the globe, with 54 over the land and 30 over the ocean surfaces, using a Bayesian inversion system (Patra et al. 2022). The flux corrections are then distributed on to a 1×1^o latitude-longitude grid based on the basis functions of 84 regions and regionally aggregated fluxes for 15 land regions (revised from 19 regions of Tian et al. 2024) and 11 ocean regions defined by Transcom 3 intercomparison project (Gurney et al. 2000) for analysis of the flux time series. Because the MIROC4-ACTM is run at about 2.8 $^o \times 2.8^o$ horizontal resolution and our inversion is solving

emissions for only 54 regions of the global land, we will only discuss emissions after aggregating the gridded emission data to 15 subcontinental scale land regions. The oceanic 30-region inversion fluxes are briefly discussed after aggregating to 11 regions.

The following equations are used to predict optimised (inversion) sources (S) and associated source error covariance matrices (C_S) constrained by observation data (D_{Obs}) and model simulation (D_{ACTM}) with regional prior mean fluxes (S_0) and prior flux error covariance matrix (C_{S0}):

$$S = S_0 + \left(G_T C_D^{-1} G + C_{S0}^{-1}\right)^{-1} G^T C_D^{-1} \left(D_{Obs} - D_{ACTM}\right) \quad (1)$$

$$C_S = \left(G_T C_D^{-1} G + C_{S0}^{-1}\right)^{-1} \quad (2)$$

C_D is the measurement data error covariance matrix. The regionally uncorrelated prior flux uncertainties and measurement data uncertainties are calculated as the square root of C_{S0} and C_D, respectively, and are represented by diagonal matrices. The C_{S0} are defined as 50% of regional total prior fluxes, and C_D are defined as (0.1 + RSD*0.3) ppb^2 (following the best case identified in Patra et al. 2022). Site specific residual standard deviations (RSD) are calculated using the curve fitting to the model simulations (Nakazawa et al. 1997). Sites close to the high emission regions received lesser weightage due to greater RSD, as mentioned in Sect. 2.1.

Prior emission cases

Inversion model estimated fluxes have large dependency on the prior flux emission distribution, particularly when the measurement network is not sufficiently dense (Fig. 1d) to capture the spatio-temporal variabilities in regional fluxes (Fig. 1c). Six different emission cases (Table 1) are formulated to test the impact of land and ocean fluxes on N_2O inversion results based on the principles described in Patra et al. (2022). The oceanic prior fluxes are available as monthly-mean and repeating between years (referred to as cyclostationary) (Yang et al. 2020) but scaled for global totals to 3.2, 3.6 and 4.2 TgN yr^{-1}. Three ocean cases are prepared to account for prior flux selection on inversion results as reflected through the 6 inversion cases. Annual mean emissions from industrial activities are taken from Emissions Database for Global Atmospheric Research, version 8 (EDGAR_v8), including sectors of fossil fuel usage, chemical industry, industrial operations, transportation systems, waste management, biomass burning (Crippa et al. 2024). Natural soil emissions are taken from a fixed annual map from Global Emissions Inventory Activity (GEIA; Bouwman et al. 2013) and the Vegetation Integrative SImulator for Trace gases (VISIT; Ito et al. 2018). Agricultural soil emissions are also taken from EDGAR_v8 (annual maps varying interannually) and VISIT. The VISIT model simulated fluxes vary monthly and interannually, driven by reanalysed climate fields and fertiliser-use information from the global N_2O Model Intercomparison Project, Phase 2 (NMIP2; Tian et al. 2018, 2024). The VISIT natural soil emissions contain effects of climate variability and agricultural soil emissions are dominantly controlled by nitrogen fertilisers, manure production and atmospheric deposition of reactive-nitrogen (N_R) on land (Ito et al. 2018).

Results and discussion

The effect of regional emission signals is variedly captured by concentrations at different sites on the globe, producing dynamic spatial gradients. We present one such development in concentration gradient change in the East Asia and Pacific Ocean regions (with an aim to elucidate the emission processes involved using numerical models). Figure 2a shows the time series of N_2O concentration, spreading over the downwind of continental East Asia (HAT: Hateruma and COI: Cape Ochi-Ishi, Japan) and remote islands in central tropical Pacific Ocean (SMO: American Samoa Observatory and MLO; Mauna Loa Observatory, USA). The growth rate time series for the period 2000 to 2023 suggest an acceleration

Table 1 List of emission combinations used in running the forward and inverse model cases. Combinations are prepared using industrial, natural soil, agricultural soil and sea-air N_2O fluxes (column 2 through 5, respectively). Global total emissions for each of the distinct sectors are given in parenthesis as average values for the decade of 2000s and 2010s, respectively, for the interannually varying emission sectors (else only one long-term mean is given; units: TgN yr^{-1}). Values in the parenthesis are not repeated for each row, if data source is identical, and only one value is listed for the emissions without interannual variability

Abbreviated name of model case	Anthropogenic industrial emissions	Natural soil emissions	Agriculture soil/fertiliser-use emissions	Ocean/ sea-air exchange
1. agey32	EDGAR_v8 (1.8, 2.0)	GEIA (7.5)	EDGAR_v8 (3.9, 4.4)	Yang_32 (3.2)
2. avey32	EDGAR_v8	VISIT(7.4, 7.5)	EDGAR_v8	Yang_32
3. agvy32	EDGAR_v8	GEIA	VISIT (3.4, 3.8)	Yang_32
4. avvy32	EDGAR_v8	VISIT	VISIT	Yang_32
5. avvy36	EDGAR_v8	VISIT	VISIT	Yang_36 (3.6)
6. avvy42	EDGAR_v8	VISIT	VISIT	Yang_42 (4.2)

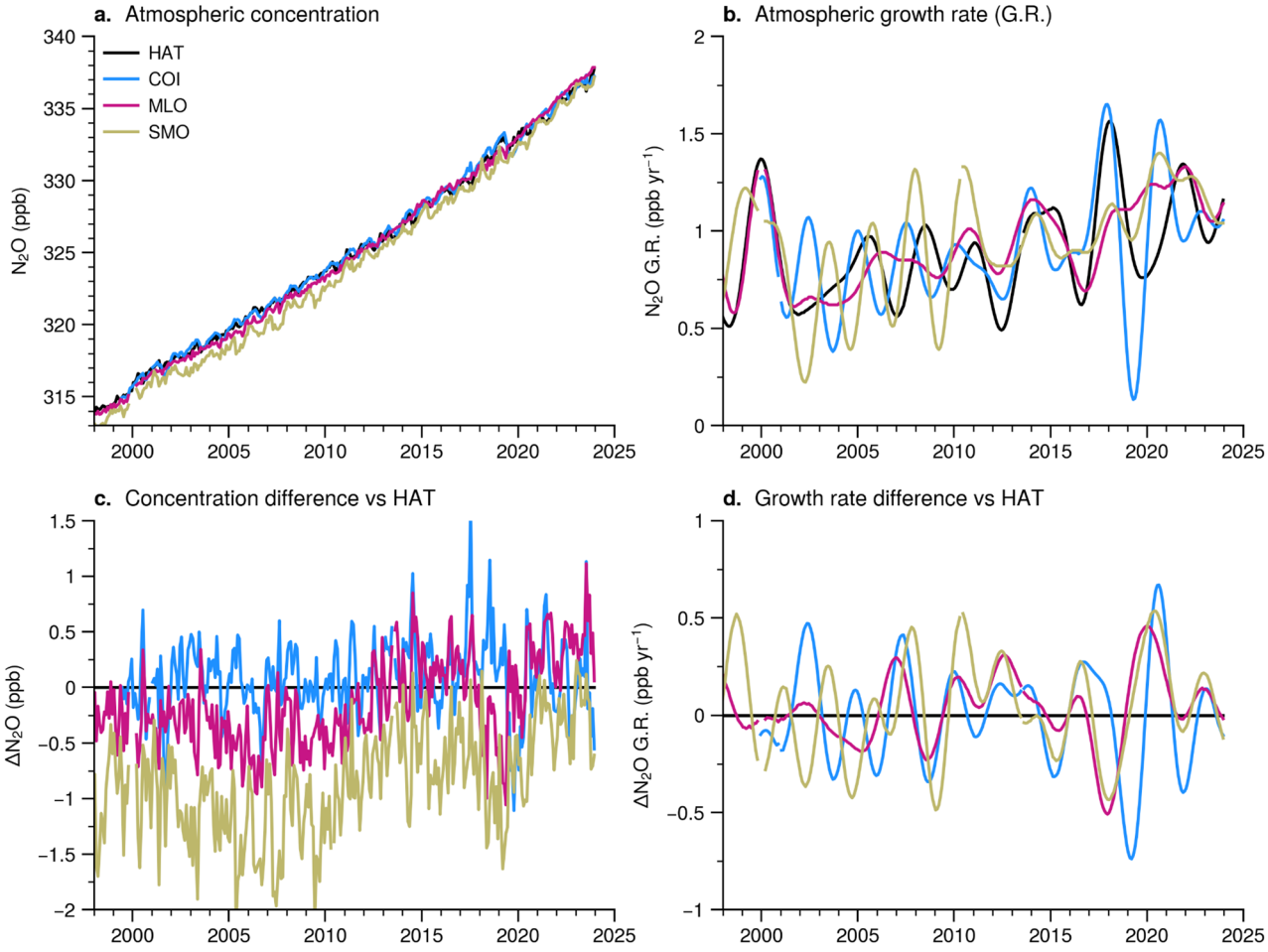


Fig. 2 The NOAA and NIES observed N_2O time series (**a**), atmospheric growth rate, G.R. (**b**), inter-site concentration gradients, ΔN_2O, with respect to HAT (**c**), and differences in growth rates (ΔN_2O G.R.) with respect to HAT (**d**) are shown for selected sites during 1998–2024. The site locations can be seen in Fig. 1, at #41 (MLO; 19.53°N,155.58°W), #44 (SMO; 14.25°S,170.57°W), #48 (COI; 43.15°N,145.50°E) and #49 (HAT; 24.05°N,123.80°E)

of the growth rate in recent times, post 2017, without any sustained differences between sites (Fig. 2b, d). One of the aims of this study is to understand the causes of large systematic changes in inter-site concentration differences/gradients (ΔN_2O), greatest between SMO - HAT, and smallest between COI - HAT and intermediate between MLO - HAT (Fig. 2c). Detection of inter-site gradients and annualised growth rates, typically below 1.5 ppb, demands extremely high precision measurements and traceability of concentrations to the calibration scale, which has been the target of the research community. Despite all the quality controls, there is some doubt about the drastic changes in NIES measurements from COI and HAT in 2019, showing a sudden drop in concentration. However, this will not affect overall conclusions of this work (Fig. S1), but is highlighted as one of the important issues that the measurement community is striving to achieve for each of the measurement points.

There is no general consensus on what should be the acceptable difference in measurement scales between the institutions and how dense a measurement network is essential for regional flux inversion. To explore this, we performed 4 additional inversions by selecting 3 sets of the measurement networks, by excluding overlapping NOAA and AGAGE sites and by excluding 2 NIES sites, and by adopting a time-dependent scale adjustment for the AGAGE sites (Fig. S1). Since the NOAA cooperative measurement network covers most parts of the globe, the inversion estimated N_2O emissions are not significantly different for the 15 land regions. The emission anomaly showed greater differences during 2012–2023 for the inversions with or without NIES sites at HAT and COI (Fig. S1i), as these sites on the western edge of Japan capture the outflow of mainland China emissions, critical for capturing the time evolution of continental fluxes (Tohjima et al. 2020). Note also that the mean of estimated N_2O emissions is fairly similar for the inversion cases with and without the NIES sites, 1.90 and 1.88 TgN yr^{-1}, respectively. However, a much greater impact of up to 0.4 TgN yr^{-1} lower N_2O emissions is found for

the East Asia region when calibration scale adjustment was not applied (Fig. S1; case: agey32_noScl). The time-dependent scale adjustment vs. fixed scale adjustment to AGAGE sites also did not produce significant difference in inversion fluxes at regional (Fig. S1) or at semi-hemispheric level (not shown). These results only reiterate the usefulness of measurement on accurate scales with inter-comparability but cannot prescribe any level of tolerance.

Since N_2O is a chemically inert species in the troposphere, the inter-site gradients in concentrations are likely to arise from the regional changes in surface fluxes, which are estimated by inverse modelling and discussed in the rest of the article. The effect of changing transport is accounted for by the transport model simulations using realistic meteorology by nudging MIROC4-ACTM meteorology to JRA-55. The N_2O growth rates are known to vary closely with El Niño Southern Oscillation (ENSO) at decadal time scales due to natural processes such as changes in soil moisture, and atmospheric transport (Fig. 2b; Ishijima et al. 2009; Nevison et al. 2007; Saikawa et al. 2014). An acceleration in the growth to ~1.0 ppb yr^{-1} has been seen during 2014–2018, compared to 0.7 ppb yr^{-1} in 2001–2005, caused by anthropogenic activities (Thompson et al. 2019), which is further intensified to 1.15 ppb yr^{-1} in 2019–2023. The difference in growth rates with respect to HAT only show interannual variability, while the mean growth rate differences are less than 0.04 ppb yr^{-1} during 1998–2023 (Fig. 4d). This uniformity in long-term mean N_2O growth rate is a result of no apparent loss on the Earth's surface or in the troposphere, and the interannual variability in growth rate differences arise from timing of regional sources variability and their transport to sites at a range of distances.

Figure 3 shows the time series of global and regional N_2O emissions using atmospheric data from 49 sites in the inversions. Long-term mean emissions for the global land are somewhat consistent for the land regions in the prior and predicted cases (Fig. 3b), while the disagreements between the prior and predicted cases are clear for the latitude bands. Most prominently, the prior emissions are systematically underestimated for the NH tropics (TrN; Fig. 3k) lands, while the prior emissions are overestimated for the Southern Hemisphere (SH; Fig. 3n) land for the period earlier than 2010. Similar to the results obtained in Patra et al. (2022), our inversion system suggests that the long-term mean oceanic emissions should be lower than 3.2 TgN yr^{-1} (3 lowest cases of ocean a priori emission) and inversions estimated the global total ocean emission to be 2.9 ± 0.15 TgN yr^{-1} (Fig. 3c). The long-term variabilities are driven by industrial and agricultural soil emissions, whereas the interannual variabilities are driven by natural soil emissions (Fig. S2).

The control of ENSO driven climate anomalies on inversion estimated N_2O flux variability is apparent for the global land (Fig. 3b), which generally show a peak following La Niña and trough following an El Niño (Thompson et al. 2014; Patra et al. 2022). The interannual flux variabilities will not be discussed in greater detail in this article and focus is given to emission change rates during different time periods and regions. However, the interannual variabilities in regional land and ocean fluxes are seen in Fig. 4 and Fig. S3, respectively, and a statistical analysis of lead-lag correlation on N_2O flux anomalies at 3-monthly mean intervals are given in Table S2. It is found that the TrN and SH land regions are the main drivers of the global N_2O emission anomaly and ENSO index variability (Table 2). Although the ocean regions also show statistically significant correlations (Table S2), the magnitude of variability in N_2O fluxes are small compared to those for the land. This is under the assumptions of the inverse model setup, e.g., the a priori flux uncertainties are set at 50% of the net emissions for all 54 land and 30 ocean regions, and the 49 sites in the observational network (ref. Sect. 2).

We find the global total emission increase occurred strongly during 2005–2018 and then stabilised at the highest level in the recent years (2018–2023). The major interannual variabilities and trends on global N_2O emissions are discussed in details later in the article. Compared to all the prior flux cases (50 ± 10 GgN yr^{-1} per year) the global land emissions increased at a much faster rate of 106 ± 5 GgN yr^{-1} per year for the inversion fluxes during the period 1998–2002 (first 5 years) and 2019–2023 (last 5 years) of analysis. The uncertainty of emission increase rates are calculated based on 6 inversion cases, and the increase rate represents the difference between mean fluxes in 1998–2002 and 2019–2023, divided by the time interval. Inversion cases only marginally, but persistently, increased N_2O emissions from global oceans (7 ± 2 GgN yr^{-1} per year), from no prior flux variability, from 1998 to 2002 to 2019–2023. This small increase in oceanic emission could arise from the deposition of N_R on ocean surfaces (e.g., Duce et al. 2008), which has remained fairly stable globally since the 1990s (Tian et al. 2024; their Fig. B3).

The origin of land flux variations and trends are found to occur from the northern hemisphere (NH) mid-high latitudes (NML; Fig. 3h), TrN (Fig. 3k) and SH (Fig. 3n) lands. However, the rate of increase in N_2O emissions varies with time from these 3 latitude bands with distinct phases of flux variability, which can explain the inter-site concentration gradient between HAT and SMO, as discussed earlier (Fig. 2c). As expected, the spread between the inversion estimated fluxes decreased for all the latitude bands, compared to the spread in 6 a priori emission cases. The SMO-HAT ΔN_2O decreased during 1998–2007 due to faster increase in emissions from the NML and TrN (5.7 ± 8.7 and 34 ± 3.3 GgN yr^{-1} per year,

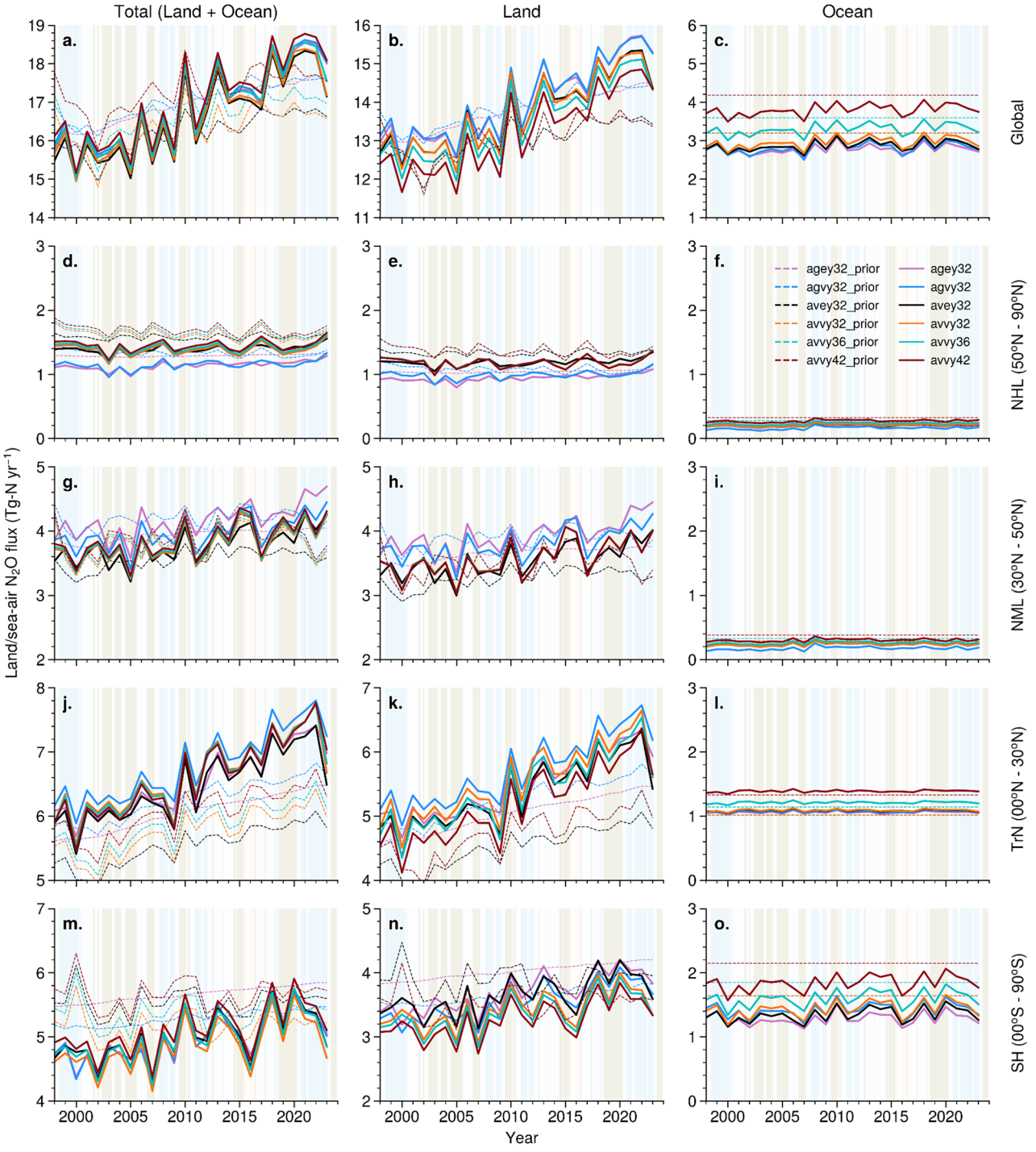


Fig. 3 Global total and semi-hemispheric N_2O flux time series of land and ocean (first column), land only (second column), and ocean only (third column) are shown at annual intervals for the period 1998–2023. Dotted lines represent prior mean flux estimates, while solid lines represent corresponding inversion-estimated fluxes. The land fluxes include both the anthropogenic (industrial + agriculture soil) and natural (soil) components. Note variable y-axis limits but a common y-axis range of 3 TgN yr^{-1} for the semi-hemispheric fluxes are used for depicting relative strength of the interannual variabilities (panels d-o). The light blue and red shades denote La Niña and El Niño periods of ENSO, respectively

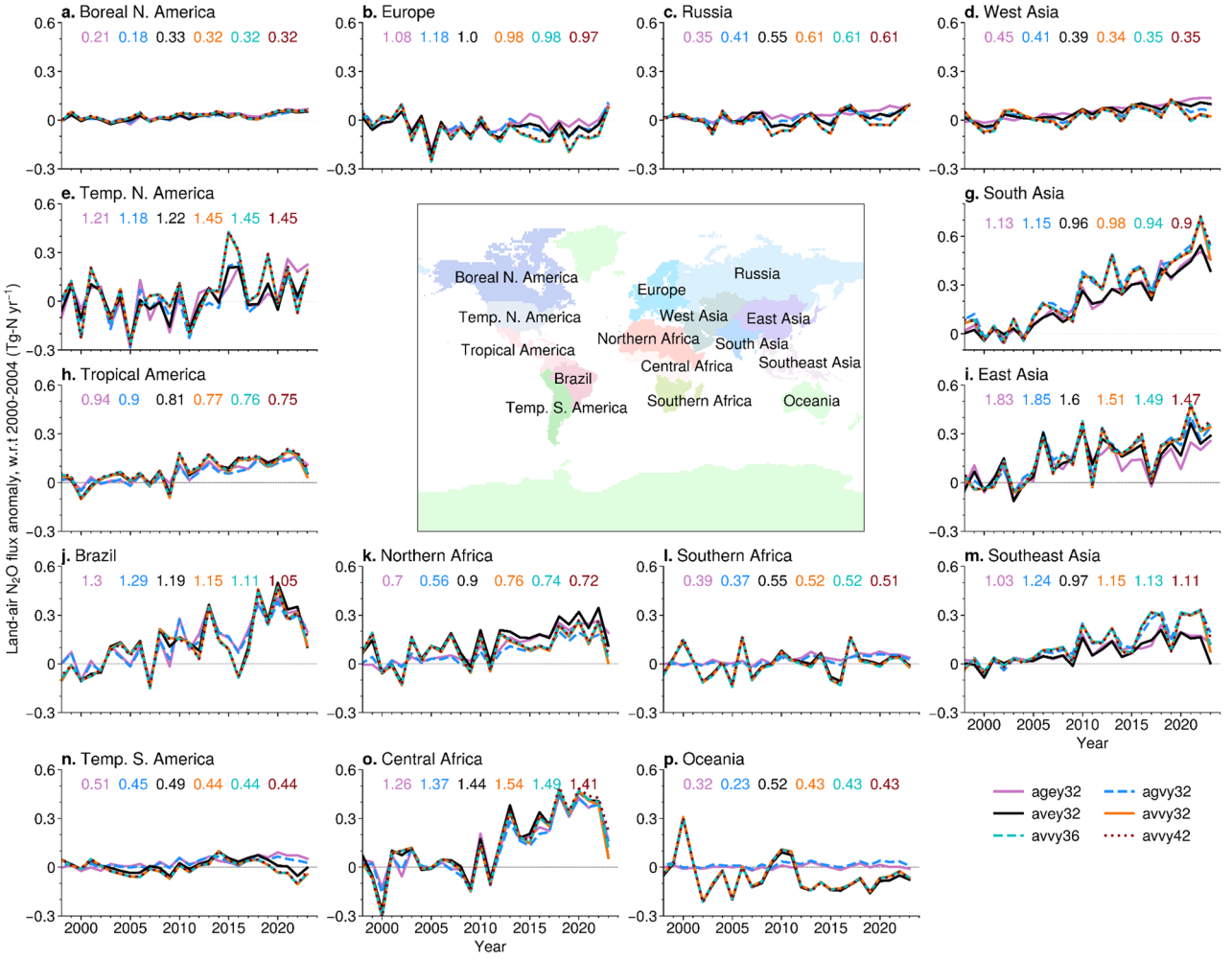


Fig. 4 Monthly time series of regional N_2O flux anomalies for the ensemble of inversions over 1998–2023 period, relative to the 2000–2004 mean. The number shown in each panel is the average for 2000–2004 for each individual inversion case. Sectoral emission anomalies for the land regions are shown in Supplementary Fig. S2. The flux anomaly time series of 11 ocean regions are shown in Supplementary Fig. S3

Table 2 Statistics of agreement between VISIT simulated natural + agricultural soil N_2O fluxes (avvy32 prior cases) with the inversion estimated flux cases (a**y32) for semi-hemispheric land divisions (ref. Fig. 3), indicating the capacity of the inverse model to retrieve N_2O flux variability and consistency of VISIT simulated fluxes with observed N_2O in the atmosphere. The N_2O emission anomaly and ENSO index correlations calculated using 3-monthly mean time intervals data (right-most column), with detailed in Table S2

Semi-hemispheric land divisions	Spearman's rank Correlation (*r*) / *p*-value of inversion cases and VISIT prior case (avvy32)				Change in emissions, (2019–2023) – (1998–2002)	*r* for mean of all 6 cases with ENSO
	agey32	agvy32	avey32	avvy32		
Global total	0.70/ 0.0001	0.72/ 0.0001	0.72/ 0.0001	0.77/ 0.0001	2.32	– 0.26
NH high latitudes (NHL)	– 0.04/ 0.84	0.45/ 0.02	0.38/ 0.051	0.78/ 0.000	– 0.02	– 0.20
NH mid-high latitudes (NML)	0.33/ 0.08	0.41/ 0.03	0.37/ 0.06	0.50/ 0.001	0.39	0.07
NH tropics (TrN)	0.84/ 0.0001	0.88/ 0.0001	0.84/ 0.0001	0.89/ 0.0001	1.35	– 0.28
SH total (SH)	– 0.09/ 0.66	0.09/ 0.63	0.49/ 0.01	0.51/ 0.01	0.59	– 0.39

respectively; Fig. 3e, k), compared to that from the SH land (1.6 ± 9 GgN yr^{-1} per year; Fig. 3n). This SMO-HAT ΔN_2O trend was reversed in the period 2007 through 2023 as the emission increase in the SH land gained faster pace (28 ± 7 GgN yr^{-1} per year), comparable to that for the NML (33 ± 12 GgN yr^{-1} per year) and TrN (74 ± 21 GgN yr^{-1} per year).

Figure 4 shows that the regional land flux anomalies exhibit large variations as well as increasing trends for the regions where agriculture is intensive, suggesting that the global use of nitrogen fertiliser and manure has grown in the past two decades. The emission anomalies for industrial anthropogenic, agricultural soils and natural soils along with the inversion ensemble means are shown in Fig. S2. The interannual variability for the tropical regions is controlled by the dominant climate variability driven by ENSO, as discussed in Patra et al. (2022, and references therein). It is noted that the VISIT model simulated (bottom-up) prior flux interannual variabilities (cases: avvy32) are generally well retrieved by the inversions (top-down) for a priori that used no interannual variability (case: agey32) at the semi-hemispheric divisions (Table 2). Such top-down and bottom-up agreements are also apparent for most of the 15 land regions (Fig. 4), the level of which defines our ability to comprehensively understand N_2O emission processes. The Oceania region fluxes using VISIT natural soil are not supported by inversions (cases: av* vs. cases: ag*; Fig. 4p), which is likely due to the fact that the Australian measurement network does not constrain the land fluxes (Haverd et al. 2013). Similar is the case with Southern Africa, where the interannual variability in VISIT natural soil is not estimated solely by inversion (Fig. 4l). It is to be acknowledged here that high quality data are available at more sites in the post-2010 period, but are excluded in the inversions as this analysis aimed to cover results since the late 1990s.

The regions with net emissions exceeding 1 TgN yr^{-1} during 2000–2004 are Europe (Fig. 4b), Temperate North America (Fig. 4e), South Asia (Fig. 4g), East Asia (Fig. 4i), Brazil (Fig. 4j), Southeast Asia (Fig. 4m) and Central Africa (Fig. 4o). Among these, only Europe showed a stable or a slightly declining trend in emissions during our analysis period (1998–2023), suggesting the use of nitrogen fertilisers and manure in the major agricultural active nations continues to grow. The other regions showing fast increasing emissions are Tropical America (Fig. 4h) and Northern Africa (Fig. 4k), with total emissions touching 1 TgN yr^{-1} in the 2020s. Figure S4 shows the net amount of nitrogen fertilisers used in each region along with the ensemble mean net N_2O emissions by inversions. The ratios of regional total (natural+anthropogenic) N_2O emissions to nitrogen fertiliser use are found to be about 0.1 for the agriculture intensive regions in the recent years (e.g., the 2020s), while the regions with a large fraction of uninhabited lands (greater fraction of natural soil) show the emission ratios exceeding 0.2 (ref. Fig. S5). Control of the fraction of nitrogen compounds released as N_2O from the agricultural soils is one of the options to reduce N_2O emissions (Shen et al. 2021; Mosier et al. 1998; Lawrence et al. 2021).

The regional N_2O emission intensity (defined by the ratio of total emissions to anthropogenic nitrogen input) is found to be stable over Europe, Temperate North America, Tropical America and West/South/East Asia, while the other 9 regions showed a reduction in the ratio during 1999–2023. The atmospheric deposition of N_R has experienced drastic changes during the period of analysis, e.g., over the United States (Zhu et al. 2025a, b), but likely to be poorly accounted in driving the global biogeochemical models (Tian et al. 2024). However, it could be argued that this drastic change in N deposition is largely driven by agricultural activities (Galloway et al. 2003; Chen et al. 2020), meaning that the temporal change in N_2O emissions is directly or indirectly attributable to the use of N fertilizers. The use of nitrogen fertilisers applied to cropland and pasture, and manure additions to cropland, pasture and rangeland have continued to rise (ref. Tian et al. 2024). In the VISIT model, about 50% of the emission increase since the early 2000s is caused by nitrogen fertiliser use, and a major part of the remaining half is caused by manure application and atmospheric N_R deposition in Asia (Ito et al. 2018). A clear separation of sector-wise emissions is not possible by our inverse model due to coarse forward and inversion model resolutions, and thus the determination of regional emission factor for nitrogen fertilisers would be overestimated if based on total regional inversion fluxes.

Figures 5 and Fig. S6 show how the regional N_2O emissions from all source sectors and nitrogen fertiliser use have changed over time, the most recent decade and over the period of the analysis, respectively. In the period from 2000 to 2004 to 2016–2020 all regions showed increased fertiliser use and thus increased N_2O emissions, except for some parts of Europe, while the maps of changes in the period from 2011 to 2013 to 2018–2020 show large regional variations. Most prominently, the nitrogen fertiliser use has decreased over China, Europe and Temperate North America (Fig. 5b). As a result, some regions of China are exhibiting decreases in N_2O emissions (Fig. 5a), with the East Asia region as a whole showing a decrease in emissions (Fig. 5c). In contrast, most parts of South Asia and temperate regions of South America show a continued increase in fertiliser and manure use and N_2O emissions in the most recent decade. Although no large increase in fertiliser use is seen over most parts of Africa, our inversion suggested large increases in emission, in particular over the tropical regions. Notably

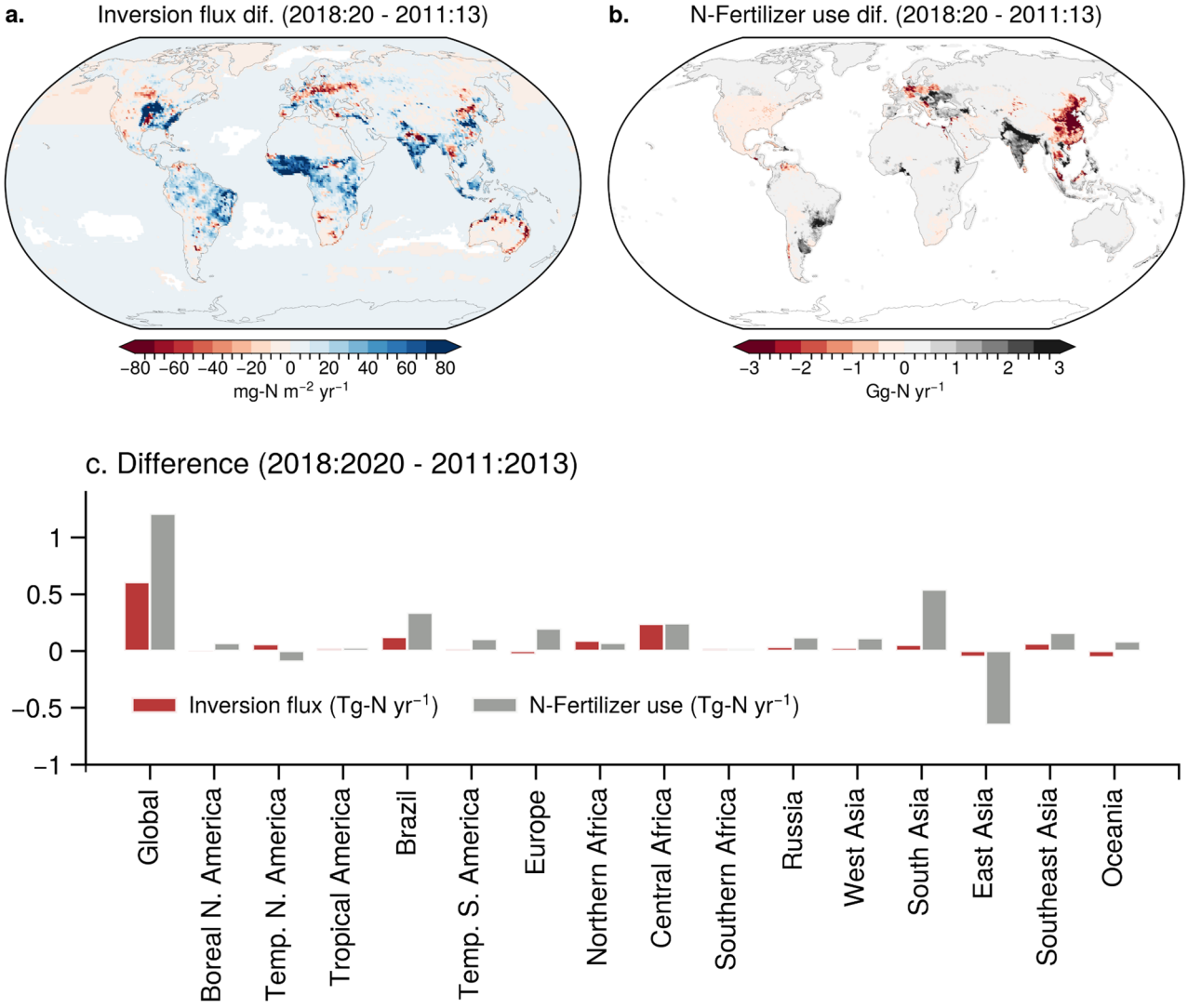


Fig. 5 The spatial maps illustrate the change in mean inversion fluxes, including all sectors (**a**) and nitrogen fertiliser applied to cropland and pasture (**b**) between the periods 2018–2020 and 2011–2013 (differences over 7 year). The bar charts (**c**) display the regional changes in fluxes, as depicted in the spatial maps above. Note that this analysis is restricted until 2020 because of the availability of N-fertilizer input data. Results for the 2016–2020 vs. 2000–2004 are shown in Fig. S6. The correlations between the differences in inverse model fluxes and nitrogen fertliser use are shown in Fig. S7

these areas of tropics are also the regions of large fraction of manure application to cropland (Tian et al. 2018). More careful separation of the natural and agricultural soil emissions must be made before we can arrive at more concrete conclusions on NUE of nitrogen-fertilisers using atmospheric inversions, including that of the cropland expansion/reduction.

Conclusions

We have performed inverse modelling of atmospheric N_2O for the period of 1998 to 2023 using measurements made by NOAA, AGAGE, CSIRO, NIES and JMA operated sites at 40 distinct locations worldwide (49 sites in total). The inverse model uses the emission inventories from EDGAR_v8, VISIT land ecosystem model, GEIA natural soil emissions, and oceanic exchange maps. Global mean N_2O has increased at the rates of 0.8 and 1.1 ppb yr^{-1} in the first (1998–2007) and final (2014–2023) decades of our analysis, respectively, with corresponding global total emissions of 15.7 ± 0.5 and 17.7 ± 0.6 TgN yr^{-1}. The increase rate of total land emissions by inversions (106 ± 5 GgN yr^{-2}) is found to be almost twice as large as those in the case of prior emissions (50 ± 10 GgN yr^{-2}), suggesting a gap in process level understanding of N_2O emissions that is required for projecting future emission scenarios. With the current prior and observational network, the observations can be reproduced without requiring large additional trends in the ocean flux.

The observations since 2010 suggest that N_2O concentration differences have lessened between HAT (24°N,

located in the emission outflow region of continental East Asia) and two tropical sites in the central Pacific Ocean (SMO; 14ºS and MLO; 19ºN). Correspondingly, the inversion modelling estimated faster increase in the NH tropical and SH lands, compared to the NH mid and high latitude lands. At the regional scales, 13 out of 15 land regions show moderate to fast increase in emissions, suggesting only the Europe and Oceania regional emissions have stayed stable in the period of our analysis. We show the increase in regional N_2O emissions are closely linked to the agricultural activities by the extensive use of nitrogen fertilisers.

Based on the VISIT ecosystem model and NMIP simulations, FAO statistics of fertiliser use, and inversion estimated regional emission trends suggest that the ratio of N_2O emission to nitrogen fertiliser use have changed over time. The N_2O emission intensity (the ratio) is found to be stable over Europe, Temperate North America, Tropical America and West/South/East Asia, while the other 9 regions showed a reduction in the ratio. In the recent decade, nitrogen fertiliser use and N_2O emissions both have stabilised or slightly decreased in East Asia, mainly due to the changes over China. Emissions of N_2O from South Asia, Southeast Asia, Brazil, and Central and Northern Africa regions showed the fastest increase in the past two decades, where the use of both nitrogen fertlisers and manure continued to rise.

Supplementary Information

The online version contains supplementary material available at https://doi.org/10.1186/s40562-026-00476-z.

Supplementary Material 1

Acknowledgements

We thank colleagues at the measurement centres for their relentless work to support experimental facilities over a long period of time. Long-term data record without major disruptions is key to perform inverse modelling of atmospheric constituents. The MIROC4-ACTM is developed and maintained by JAMSTEC (Dr. M. Takigawa), and simulations are run on Earth Simulator, generation 4 (ES4). This work was presented at the AOGS annual meeting, Singapore, 2025.

Author contributions

P.K.P. developed the research, performed inversion calculation, and organised the manuscript draft. Y.T and P.K.P developed initial ideas of this analysis; N.C. supported data analysis and plotting; A.I. conducted VISIT model simulation; X.L., B.D.H., Y.T., M.S., R.G.P., R.F.W., C.H., P.B.K. and S.T. have contributed measurements of N 2 O, and provided the details of inter-institution calibration scales. B.D.H. led the WMO Round Robin Activity for measurement scales, with support from S.T., Y.T., R.F.W. and others. All authors (P.K.P., Y.T, A.I., N.C., M.S., X.L., B.D.H., P.B.K., R.F.W., C.M.H., D.G., K.T., L.W.) supported the writing of the manuscript draft and reviewed the final version.

Funding

This work is funded by the Environment Research and Technology Development Fund (JPMEERF24S12200) of the Environmental Restoration and Conservation Agency of Japan, and partially supported by the Arctic Challenge for Sustainability 3 (ArCS-3), Program Grant Number JPMXD1720251001. The five AGAGE stations used here are supported by the National Aeronautics and Space Administration (NASA) (grants 80NSSC21K1210 and 80NSSC21K1201 for SIO/UCSD and 80NSSC21K1369 for MIT). Support also comes from the UK Department for Business, Energy & Industrial Strategy (BEIS) for Mace Head, the National Oceanic and Atmospheric Administration (NOAA) for Barbados, and the Commonwealth Scientific and Industrial Research Organization (CSIRO) and the Bureau of Meteorology (Australia) for Kennaook/Cape Grim. CSIRO N_2O flask measurements are supported by CSIRO. NOAA N_2O measurements are supported in part by the NOAA cooperative agreement NA22OAR4320151. The statements, findings, conclusions, and recommendations are those of the author(s) and do not necessarily reflect the views of NOAA or the U.S. Department of Commerce.

Data availability

The N 2 O inversion dataset generated and analysed in the current study are available in the Zenodo repository [https://doi.org/10.5281/zenodo.14533031]. VISIT ecosystem model simulation of N 2 O flux are available at : ZenodoEDGAR_v7 data are available at: [https://edgar.jrc.ec.europa.eu/dataset_ghg80](https:/edgar.jrc.ec.europa.eu/dataset_ghg80)The processed datasets are also available from the corresponding author on reasonable request.

Declaration

Competing interests

The authors declare no competing interests.

Author details

[1]Research Institute for Global Change, JAMSTEC, Yokohama 236-0001, Japan
[2]Seto Inland Sea Carbon Neutral Research Center, Hiroshima University, Hiroshima 739-8529, Japan
[3]Research Institute for Humanity and Nature (RIHN), Kyoto 603-8047, Japan
[4]Earth System Division, National Institute for Environmental Studies (NIES), Tsukuba 305-8506, Japan
[5]Graduate School of Agricultural and Life Sciences, The University of Tokyo, Tokyo 113-8657, Japan
[6]Global Monitoring Laboratory, National Oceanic & Atmospheric Administration (NOAA), Boulder, CO 80305, USA
[7]Cooperative Institute for Research in Environmental Sciences, University of Colorado Boulder, Boulder, CO 80309, USA
[8]CSIRO Environment, Aspendale, VIC 3195, Australia
[9]Scripps Institution of Oceanography, University of California, San Diego, CA 92093, USA
[10]Atmospheric Environment and Ocean Division, Atmosphere and Ocean Department, Japan Meteorological Agency (JMA), Tokyo 105-8431, Japan
[11]National Institute of Polar Research, Tachikawa 190-8518, Tokyo, Japan
[12]Center for Sustainability Science and Strategy, Massachusetts Institute of Technology, Cambridge, MA 02139, USA
[13]Azabu University, Sagamihara 252-5201, Japan

Received: 17 September 2025 / Accepted: 30 March 2026
Published online: 28 April 2026

References

Bisht JSH, Machida T, Chandra N, Tsuboi K, Patra P, Umezawa T, Niwa Y, Sawa Y, Morimoto S, Nakazawa T (2021) Seasonal variations of SF6, CO_2, CH_4, and N_2O in the UT/LS region due to emissions, transport, and chemistry. J Geophy Res Atmos 126:e2020JD033541. https://doi.org/10.1029/2020JD033541

Bouwman AF, Beusen AHW, Griffioen J, Van Groenigen JW, Hefting MM, Oenema O, Van Puijenbroek PJTM, Seitzinger S, Slomp CP, Stehfest E (2013) Global trends and uncertainties in terrestrial denitrification and N_2O emissions. Philos Trans Roy Soc Lond Ser B 368:20130112. https://doi.org/10.1098/rstb.2013.0112

Burkholder JB, Hodnebrog Ø (2023) Summary of Abundances, Lifetimes, ODPs, REs, GWPs, and GTPs. In: Scientific assessment of ozone depletion: 2022, world meteorological organization, Geneva, Switzerland, ISBN 978-9914-733-97-6

Butterbach-Bahl K, Baggs L, Dannenmann M, Kiese R, Zechmeister-Boltenstern S (2013) Nitrous oxide emissions from soils: How well do we understand the processes and their controls? Philos Trans Roy Soc Lond Ser B 368:20130122. https://doi.org/10.1098/rstb.2013.0122

Canadell JG, Monteiro PMS, Costa MH, Cotrim da Cunha L, Cox PM, Eliseev AV, Henson S, Ishii M, Jaccard S, Koven C, Lohila A, Patra PK, Piao S, Rogelj J, Syampungani S, Zaehle S, Zickfeld K (2021) Global Carbon and other Biogeochemical Cycles and Feedbacks. Climate Change 2021: The Physical Science Basis. Contribution of Working Group I to the Sixth Assessment Report of the Intergovernmental Panel on Climate Change [Masson-Delmotte. V., et al. (eds.)]. Cambridge University Press, Cambridge, United Kingdom and New York, NY, USA, pp 673–816. doi:https://doi.org/10.1017/9781009157896.007

Chen Y, Shen H, Shih J-S, Russell AG, Shao S, Hu Y, Odman MT, Nenes A, Pavur GK, Zou Y, Chen Z, Smith RA, Burtraw D, Driscoll CT (2020) Greater contribution from agricultural sources to future reactive nitrogen deposition in the United States. Earths Future. https://doi.org/10.1029/2019EF001453

Crippa M, Guizzardi D, Pagani F, Banja M, Muntean M, Schaaf E, Monforti-Ferrario F, Becker W, Quadrelli R, Martin R, Taghavi-Moharamli A, Köykkä P, Grassi J, Rossi G, Melo S, Oom J, Branco D, San-Miguel A, Manca J, Pisoni G, Vignati E, Pekar E (2024) F., GHG emissions of all world countries, vol JRC138862. Publications Office of the European Union, Luxembourg. https://doi.org/10.2760/4002897

Cui X, Zhou F, Ciais P, Davidson EA, Tubiello FN, Niu X, Ju X, Canadell JG, Bouwman AF, Jackson RB, Mueller ND, Zheng X, Kanter DR, Tian H, Adalibieke W, Bo Y, Wang Q, Zhan X, Zhu D (2021) Global mapping of crop-specific emission factors highlights hotspots of nitrous oxide mitigation. Nat Food 2(11):886–893. https://doi.org/10.1038/s43016-021-00384-9

Del Grosso SJ, Ogle SM, Nevison C, Gurung R, Parton WJ, Wagner-Riddle C, Williams S (2022) A gap in nitrous oxide emission reporting complicates long-term climate mitigation. Proc Natl Acad Sci 119(31):e2200354119

Duce RA, LaRoche J, Altieri K, Arrigo KR, Baker AR, Capone DG et al (2008) Impacts of atmospheric anthropogenic nitrogen on the open ocean. Science 320:893–897. https://doi.org/10.1126/science.1150369

Forster P, Storelvmo T, Armour K, Collins W, Dufresne J-L, Frame D, Lunt DJ, Mauritsen T, Palmer MD, Watanabe M, Wild M, Zhang H (2021) The Earth's Energy Budget, Climate Feedbacks, and Climate Sensitivity. Climate Change 2021: The Physical Science Basis. Contribution of Working Group I to the Sixth Assessment Report of the Intergovernmental Panel on Climate Change [Masson-Delmotte,V. et al. (eds.)]. Cambridge University Press, Cambridge, United Kingdom and New York, NY, USA, pp 923–1054. doi:https://doi.org/10.1017/9781009157896.009

Galloway JN, Aber JD, Erisman JW, Seitzinger SP, Howarth RW, Cowling EB, Cosby BJ (2003) nitrogen cascade Bioscience 53:341–356. https://doi.org/10.1641/0006-3568(2003)053[0341:TNC]2.0.CO;2

Gurney K, Law R, Rayner P, Denning AS (2000) TransCom 3 experimental protocol, Pap. 707, Dept. of Atmos. Sci., Colo. State Univ., https://www.researchgate.net/publication/228955926_TransCom_3_Experimental_Protocol (last accessed: 09 September 2025)

Hall BD, Dutton GS, Elkins JW (2007) The NOAA nitrous oxide standard scale for atmospheric observations. J Geophys Res 112:D09305. https://doi.org/10.1029/2006JD007954

Harris E, Yu L, Wang Y-P, Mohn J, Henne S, Bai E, Barthel M, Bauters M, Boeckx P, Dorich C, Farrell M, Krummel PB, Loh ZM, Reichstein M, Six J, Steinbacher M, Wells NS, Bahn M, Rayner P (2022) Warming and redistribution of nitrogen inputs drive an increase in terrestrial nitrous oxide emission factor. Nat Commun 13(1):4310. https://doi.org/10.1038/s41467-022-32001-z

Haverd V, Raupach MR, Briggs PR, Canadell. JG, Davis SJ, Law RM, Meyer CP, Peters GP, Pickett-Heaps C, Sherman B (2013) The Australian terrestrial carbon budget. Biogeosciences 10:851–869. https://doi.org/10.5194/bg-10-851-2013

Huang J, Golombek A, Prinn R, Weiss R, Fraser P, Simmonds P, Dlugokencky EJ, Hall B, Elkins J, Steele P, Langenfelds R, Krummel P, Dutton G, Porter L (2008) Estimation of regional emissions of nitrous oxide from 1997 to 2005 using multinetwork measurements, a chemical transport model, and an inverse method. J Geophys Res 113:D17313. https://doi.org/10.1029/2007JD009381

Ishijima K, Nakazawa T, Aoki S (2009) Variations of atmospheric nitrous oxide concentration in the northern and western Pacific. Tellus B 61:408–415. https://doi.org/10.1111/j.1600-0889.2008.00406.x

Ito A, Nishina K, Ishijima K, Hashimoto S, Inatomi M (2018) Emissions of nitrous oxide (N_2O) from soil surfaces and their historical changes in East Asia: a model-based assessment. Progress Earth Planet Sci 5:55. https://doi.org/10.1186/s40645-018-0215-4

Kobayashi S, Ota Y, Harada Y, Ebita A, Moriya M, Onoda H, Onogi K, Kamahori H, Kobayashi C, Endo H, Miyaoka K, Takahashi K (2015) The JRA-55 Reanalysis: general specifications and basic characteristics. J Meteor Soc Japan 93:5–48. https://doi.org/10.2151/jmsj.2015-001

Lan X, Mund JW, Crotwell AM, Mauss J, Madronich M, Moglia E, Baugh K, Searle A, Petron G, Crotwell MJ, Mefford T, DeVogel S, Wolter S, Thoning KW, Morris S, Miller J (2024) Atmospheric nitrous oxide dry air mole fractions from the NOAA GML carbon cycle cooperative global air sampling network, starting in 1997, Version: 2024-07-30. https://doi.org/10.15138/53g1-x417

Lan X, Thoning KW (2025) Dlugokencky EJ Trends in globally-averaged CH_4, N_2O, and SF_6 determined from NOAA global monitoring laboratory measurements. https://doi.org/10.15138/P8XG-AA10

Lawrence NC, Tenesaca CG, VanLoocke A, Hall SJ (2021) Nitrous oxide emissions from agricultural soils challenge climate sustainability in the US Corn Belt. Proc Natl Acad Sci U S A 118(46):e2112108118. https://doi.org/10.1073/pnas.2112108118

Li L, Lu C, Winiwarter W, Tian H, Canadell JG, Ito A, Jain AK, Kou-Giesbrecht S, Pan S, Pan N, Shi H, Sun Q, Vuichard N, Ye S, Zaehle S, Zhu Q (2024) Enhanced nitrous oxide emission factors due to climate change increase the mitigation challenge in the agricultural sector. Glob Change Biol 30:e17472. https://doi.org/10.1111/gcb.17472

Mosier A, Duxbury J, Freney J, Heinemeyer O, Minami K (1998) Assessing and Mitigating N_2O Emissions from Agricultural Soils. Clim Change 40:7–38. https://doi.org/10.1023/A:1005386614431

Nakazawa T, Ishizawa M, Higuchi K, Trivett NBA (1997) Two curve fitting methods applied to CO2 flask data. Environmetrics 8:197–218. https://doi.org/10.1002/(SICI)1099-095X(199705)8:3%3C197::AID-ENV248%3E3.0.CO;2-C

Nevison CD, Mahowald NM, Weiss RF, Prinn RG (2007) Interannual and seasonal variability in atmospheric N_2O, Global Biogeochem. Cycles 21:GB3017. https://doi.org/10.1029/2006GB002755

Patra PK, Dlugokencky EJ, Elkins JW, Dutton GS, Tohjima Y, Sasakawa M, Takigawa M (2022) Forward and inverse modelling of atmospheric nitrous oxide using MIROC4-atmospheric chemistry-transport model. Journal of the Meteorological Society of Japan 100(2):361–386

Patra PK, Takigawa M, Watanabe S, Chandra N, Ishijima K, Yamashita Y (2018) Improved chemical tracer simulation by MIROC4.0-based atmospheric chemistry-transport model (MIROC4-ACTM). Sola 14:91–96. https://doi.org/10.2151/sola.2018-016

Patra PK, Patra PK, Dlugokencky EJ, Elkins JW, Dutton GS, Tohjima Y, Sasakawa M, Ito A, Weiss RF, Manizza M, Krummel PB (2024) Forward and inverse modelling of atmospheric nitrous oxide using MIROC4-atmospheric chemistry-transport model. J Meteorol Soc Japan Ser II 100:361–386. https://doi.org/10.2151/jmsj.2022-018

Porporato A, Laio F, Ridolfi L, Caylor KK, Rodriguez-Iturbe I (2003) Soil moisture and plant stress dynamics along the Kalahari precipitation gradient. J Geophys Res Atmos 108:4127. https://doi.org/10.1029/2002JD002448

Prather MJ, Hsu J, DeLuca NM, Jackman CH, Oman LD, Douglass AR, Fleming EL, Strahan SE, Steenrod SD, Søvde OA, Isaksen ISA, Froidevaux L, Funke B (2015) Measuring and modeling the lifetime of nitrous oxide including its variability. J Geophys Res Atmos 120:5693–5705. https://doi.org/10.1002/2015JD023267

Prinn RG, Weiss RF, Arduini J, Arnold T, DeWitt HL, Fraser PJ, Ganesan AL, Gasore J, Harth CM, Hermansen O, Kim J, Krummel PB, Li S, Loh ZM, Lunder CR, Maione M, Manning AJ, Miller BR, Mitrevski B, Mühle J, O'Doherty S, Park S, Reimann S, Rigby M, Saito T, Salameh PK, Schmidt R, Simmonds PG, Steele LP, Vollmer MK, Wang RH, Yao B, Yokouchi Y, Young D, Zhou L (2018) History of chemically and radiatively important atmospheric gases from the Advanced Global Atmospheric Gases Experiment (AGAGE). Earth Syst Sci Data 10:985–1018. https://doi.org/10.5194/essd-10-985-2018

Rubino M, Etheridge DM, Thornton DP, Howden R, Allison CE, Francey RJ, Langenfelds RL, Steele LP, Trudinger CM, Spencer DA, Curran MAJ, van Ommen TD, Smith AM (2019) Revised records of atmospheric trace gases CO_2, CH_4, N_2O, and $\delta^{13}C$-CO_2 over the last 2000 years from Law Dome, Antarctica. Earth Syst Sci Data 11:473–492. https://doi.org/10.5194/essd-11-473-2019

Saikawa E, Prinn RG, Dlugokencky E, Ishijima K, Dutton GS, Hall BD, Langenfelds R, Tohjima Y, Machida T, Manizza M, Rigby M, O'Doherty S, Patra PK, Harth CM, Weiss RF, Krummel PB, van der Schoot M, Fraser PJ, Steele LP, Aoki S, Nakazawa T, Elkins JW (2014) Global and regional emissions estimates for N. Atmos Chem Phys 2O:14, 4617–4641. https://doi.org/10.5194/acp-14-4617-2014

Shen H, Shiratori Y, Ohta S et al (2021) Mitigating N_2O emissions from agricultural soils with fungivorous mites. ISME J 15:2427–2439. https://doi.org/10.1038/s41396-021-00948-4

Takatsuji S (2025) Atmospheric N_2O at Ryori by Japan Meteorological Agency, dataset published as N2O_RYO2012_surface-insitu_JMA_data1 at WDCGG, ver.2025-07-31-2347. https://doi.org/10.50849/WDCGG_0001-2012-1003-01-01-9999

Thompson RL, Chevallier F, Crotwell AM, Dutton G, Langenfelds RL, Prinn RG, Aoki S (2014) Nitrous oxide emissions 1999 to 2009 from a global atmospheric

inversion. Atmos Chem Phys 14(4):1801–1817. https://doi.org/10.5194/acp-14-1801-2014

Thompson RL, Lassaletta L, Patra PK, Wilson C, Wells KC, Gressent A, Koffi EN, Chipperfield MP, Winiwarter W, Davidson EA (2019) Acceleration of global N_2O emissions seen from two decades of atmospheric inversion. Nat Clim Chang 9(12):993–998. https://doi.org/10.1038/s41558-019-0613-7

Tian H, Yang J, Lu C, Xu R, Canadell JG, Jackson RB, Arneth A, Chang J, Chen G, Ciais P, Gerber S, Ito A, Huang Y, Joos F, Lienert S, Messina P, Olin S, Pan S, Peng C, Saikawa E, Thompson RL, Vuichard N, Winiwarter W, Zaehle S, Zhang B, Zhang K, Zhu (2018) Q, The global N_2O model intercomparison project. Bull Am Meteorol Soc 99(6):1231–1251. https://doi.org/10.1175/BAMS-D-17-0212.1

Tian H, Pan N, Thompson RL, Canadell JG, Suntharalingam P, Regnier P, Davidson EA, Prather M, Ciais P, Muntean M, Pan S, Winiwarter W, Zaehle S, Zhou F, Jackson RB, Bange HW, Berthet S, Bian Z, Bianchi D, Bouwman AF, Buitenhuis ET, Dutton G, Hu M, Ito A, Jain AK, Jeltsch-Thömmes A, Joos F, Kou-Giesbrecht S, Krummel PB, Lan X, Landolfi A, Lauerwald R, Li Y, Lu C, Maavara T, Manizza M, Millet DB, Mühle J, Patra PK, Peters GP, Qin X, Raymond P, Resplandy L, Rosentreter JA, Shi H, Sun Q, Tonina D, van der Tubiello FN, Vuichard N, Wang J, Wells KC, Western LM, Wilson C, Yang J, Yao Y, You Y, Zhu Q (2024) Global nitrous oxide budget (1980–2020). Earth Syst Sci Data 16:2543–2604. https://doi.org/10.5194/essd-16-2543-2024

Tohjima Y, Patra PK, Niwa Y, Mukai H, Sasakawa M, Machida T (2020) Detection of fossil-fuel CO2 plummet in China due to COVID-19 by observation at Hateruma. Sci Rep 10:18688. https://doi.org/10.1038/s41598-020-75763-6

Tubiello FN, Karl K, Flammini A, Gütschow J, Obli-Laryea G, Conchedda G, Pan X, Qi SY, Halldórudóttir Heiðarsdóttir H, Wanner N, Quadrelli R, Souza R, Benoit L, Hayek P, Sandalow M, Mencos D, Contreras E, Rosenzweig C, Moncayo R, Conforti J, Torero P (2022) Pre- and post-production processes increasingly dominate greenhouse gas emissions from agri-food systems. Earth Syst Sci Data 14:1795–1809. https://doi.org/10.5194/essd-14-1795-2022

United Nations Environment Programme (UNEP) and Food and Agriculture Organization (FAO) of the United Nations, Global Nitrous Oxide Assessment, Nairobi (2004). Last Accessed 27 August 2025 https://openknowledge.fao.org/handle/20.500.14283/cd3298en

Vitousek PM, Aber JD, Howarth RW, Likens GE, Matson PA, Schindler DW, Schlesinger WH, Tilman DG (1997) Human alteration of the global nitrogen cycle: sources and consequences. Ecol Appl 7(3):737–750. https://doi.org/10.1890/1051-0761(1997)007[0737:HAOTGN]2.0.CO;2

Watanabe S, Hajima T, Sudo K, Nagashima T, Takemura T, Okajima H, Nozawa T, Kawase H, Abe M, Yokohata T, Ise T, Sato H, Kato E, Takata K, Emori S, Kawamiya M (2010) MIROC-ESM: model description and basic results of CMIP5-20c3m experiments. Geosci Model Dev 4:845–872. https://doi.org/10.5194/gmd-4-845-2011

World Meteorological Organization (WMO), Scientific Assessment of Ozone Depletion (SAOD): 2022, GAW Report No. 278, 509 pp.; WMO: Geneva, 2023. https://library.wmo.int/zh/records/item/42105-scientific-assessment-of-ozone-depletion-2022-executive-summary (last accessed 16 September 2025)

Yang S, Chang BX, Warner MJ, Weber TS, Bourbonnais AM, Santoro AE, Kock A, Sonnerup RE, Bullister JL, Wilson ST, Bianchi D (2020) Global reconstruction reduces the uncertainty of oceanic nitrous oxide emissions and reveals a vigorous seasonal cycle. Proc Natl Acad Sci U S (PNAS) 117:11954–11960. https://doi.org/10.1073/pnas.1921914117

Zhu G, Shi H, Zhong L et al (2025a) Nitrous oxide sources, mechanisms and mitigation. Nat Rev Earth Environ 6:574–592. https://doi.org/10.1038/s43017-025-00707-5

Zhu J, Jia Y, Yu G, Wang Q, He N, Chen Z, He H, Zhu X, Li P, Zhang F, Liu X, Goulding K, Fowler D, Vitousek P (2025b) Changing patterns of global nitrogen deposition driven by socio-economic development. Nat Commun 16:46. https://doi.org/10.1038/s41467-024-55606-y

Publisher's note

Springer Nature remains neutral with regard to jurisdictional claims in published maps and institutional affiliations.

Bradley D. Hall (retired from NOAA)